J. Fluid Mech. (1997), *vol.* 342, *pp.* 315–334. Printed in the United Kingdom

On the extinction limit and flammability limit of non-adiabatic stretched methane–air premixed flames

By YIGUANG JU[1], HONGSHENG GUO[2], KAORU MARUTA[2] AND FENGSHAN LIU[3]

[1]Department of Aeronautics and Space Engineering, Tohoku University, Aramaki Aoba, Aoba-ku, Sendai 980, Japan

[2]Institute of Fluid Science, Tohoku University, Katahira 2-1-1, Sendai 980-77, Japan

[3]Centre for Advanced Gas Combustion Technology, Department of Chemical Engineering, Queen's University at Kingston, Ontario, K7L3N6 Canada

(Received 26 July 1996 and in revised form 17 February 1997)

Extinction limits and the lean flammability limit of non-adiabatic stretched premixed methane–air flames are investigated numerically with detailed chemistry and two different Planck mean absorption coefficient models. Attention is paid to the combined effect of radiative heat loss and stretch at low stretch rate. It is found that for a mixture at an equivalence ratio lower than the standard lean flammability limit, a moderate stretch can strengthen the combustion and allow burning. The flame is extinguished at a high stretch rate due to stretch and is quenched at a low stretch rate due to radiation loss. A O-shaped curve of flame temperature versus stretch rate with two distinct extinction limits, a radiation extinction limit and a stretch extinction limit respectively on the left- and right-hand sides, is obtained. A C-shaped curve showing the flammability limit of the stretched methane–air flame is obtained by plotting these two extinction limits in the mixture strength coordinate. A good agreement is shown on comparing the predicted results with the experimental data. For equivalence ratio larger than a critical value, it is found that the O-shaped temperature curve opens up in the middle of the stable branch, so that the stable branch divides into two stable flame branches; a weak flame branch and a normal flame branch. The weak flame can survive between the radiation extinction limit and the opening point (jump limit) while the normal flame branch can survive from its stretch extinction limit to zero stretch rate. Finally, a G-shaped curve showing both extinction limits and jump limits of stretched methane–air flames is presented. It is found that the critical equivalence ratio for opening up corresponds to the standard flammability limit measured in microgravity. Furthermore, the results show that the flammability limit (inferior limit) of the stretched methane–air flame is lower than the standard flammability limit because flames are strengthened by a moderate stretch at Lewis number less than unity.

1. Introduction

The structures and extinction limits of premixed flames have been of primary interest to the combustion community. Understanding of the structure and extinction mechanism of premixed flames is frequently based on the study of one-dimensional

planar propagating flames and counterflow premixed flames. It has been well established that both radiative heat loss and flame stretch can greatly affect the structure and extinction limit of laminar flames. For one-dimensional planar propagating flames, extensive experimental and theoretical studies (Egerton & Thabet 1952; Spalding 1957; Lakshmisha, Paul & Mukunda 1990) have shown that extinction can be caused by radiation heat loss. On the other hand, experimental studies of counterflow premixed flames has revealed that they can be extinguished only by increasing the stretch rate (Tsuji 1983). The combined effect of radiation heat loss and stretch on the flame structure and extinction have also been extensively studied by investigating counterflow diffusion flames and premixed flames. For diffusion flames, Tien (1986), Liu & Rogg (1991) and Chao, Law & Tien (1990) examined the effects of radiation heat loss on flame structure at low stretch rates. Tien's study showed that there exists a radiation extinction limit at low stretch, in addition to the stretch induced extinction limit.

Compared to diffusion flames, few studies have been conducted on the structure and extinction of premixed flames at low stretch rate. Although several theoretical and experimental studies (Sohrab & Law 1984; Liu, Ye & Sohrab 1986) have been carried out to investigate the effects of radiation on stretched flames, the combined effects of radiative heat loss and stretch at low stretch rate have not been particularly addressed. Based on their theoretical study, Sohrab & Law (1984) concluded that radiative heat loss is unimportant in affecting flame extinction compared to flame stretch. In the experimental study of Liu *et al.* (1986), the stretch rate was fixed at 10 s^{-1} due to experimental difficulties of achieving lower stretch rates. Therefore, the detailed flame structure and extinction mechanism associated with the interaction between the radiation effect and the stretch effect at low stretch rate were not examined in their experiments.

Recently, the determination of the absolute flammability limit in microgravity has received great attention (Ronney 1988). Understanding of the extinction mechanism at low stretch rate and the relation between the counterflow flame and the planar propagating flame is crucial to the accurate determination of the flammability limit from the results of stretched flames. Experimental measurements (Ronney & Wachman 1985) and numerical predictions (Sibulkin & Frendi 1990) using spherically propagating flames in the absence of gravity showed that radiation heat loss produces a lean flammability limit at low stretch rates. On the other hand, to understand the essence of the extinction mechanism of counterflow flames at low stretch rates, a numerical study based on the one-step overall reaction and constant transport properties has been conducted by Platt & Tien (1990). Their results showed that there also exists a radiation extinction limit at low stretch rate. A recent experiment in microgravity (Maruta *et al.* 1996) clearly showed that a premixed flame near the flammability limit is extinguished at two different stretch rates. A numerical study conducted by the same group (Guo *et al.* 1996) with detailed chemistry and transport properties confirmed that flame extinction at low stretch rate is attributed to radiative heat loss but extinction at large stretch rate is caused by the stretch effect which has been extensively studied previously (Tsuji 1983; Sohrab & Law 1984). However, the studies by Maruta *et al.* and Guo *et al.* are confined to the extinction of flames near the lean limit. Flame structures and extinction phenomena at higher equivalence ratio have not been examined. Furthermore, the relation between the flammability limit determined from counterflow premixed flames and that of planar propagating flames still remains unknown. To obtain the flammability limit in the zero stretch limit from the results of stretched flames, a linear extrapolation method has been proposed by Law & Egolfopoulos (1990). However, recent theoretical and numerical studies (Tien

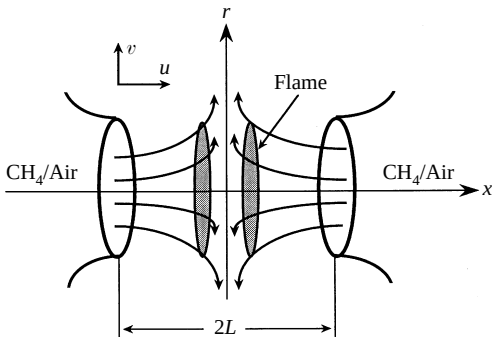

FIGURE 1. Schematic graph of the computation model.

& Matalon 1991; Dixon-Lewis 1990) indicate that the strict linear relation is not valid. The most important reason for these conflicting results is that the behaviour of premixed flames at very low stretch rates is not yet properly understood.

One objective of this study is to investigate numerically the flame regimes and extinction mechanisms of stretched lean methane–air premixed flames with detailed chemistry at low stretch rate over a wide range of equivalence ratio. The combined effect of the Lewis number and the radiation heat loss is emphasized. Another motivation is to ascertain whether the linear extrapolation from the stretch extinction limits of stretched flames to the flammability limit of zero stretch flames is valid or not. Comparisons of peak flame temperature and extinction limits between adiabatic flames and non-adiabatic flames are also made. A radiation distribution function is introduced to evaluate the quantitative effect of radiative heat loss. Then, the correlations between peak flame temperature and stretch rate for various equivalence ratios are presented. Finally, a G-shaped extinction curve is obtained and discussed.

2. Theoretical model

The flame configuration analysed in this study is the axisymmetrical counterflow laminar premixed flame shown in figure 1. Twin flames are formed near the stagnation plane of the two opposed methane–air flows. In this study, the distance between the two burners is fixed at 10 cm for all the calculations except in the comparison of temperature dips between prediction and experiment in the next section. Only one half of the domain is solved due to the symmetry of this twin flame configuration. By making the stagnation point flow approximation (Giovangigli & Smooke 1987; Kee *et al.* 1988), the governing equations can be written as

$$\left.\begin{aligned}
&\mathrm{d}a/\mathrm{d}t = 0,\\
&\frac{\mathrm{d}\rho}{\mathrm{d}t} + \frac{\mathrm{d}U}{\mathrm{d}x} = -2\rho G,\\
&\mathrm{L}(G) = \frac{\mathrm{d}}{\mathrm{d}x}\left(\mu\frac{\mathrm{d}G}{\mathrm{d}x}\right) - \rho G^2 + \rho\left(\frac{\mathrm{d}a}{\mathrm{d}t} + a^2\right),\\
&C_p\mathrm{L}(T) = \frac{\mathrm{d}}{\mathrm{d}x}\left(\lambda\frac{\mathrm{d}T}{\mathrm{d}x}\right) - \sum_{k=1}^{n}\rho Y_k V_k C_{pk}\frac{\mathrm{d}T}{\mathrm{d}x} - \sum_{k=1}^{n} h_k\dot{\omega}_k M_k + \dot{q}_r,\\
&\mathrm{L}(Y_k) = -\frac{\mathrm{d}}{\mathrm{d}x}(\rho Y_k V_{kx}) + \sum_{k=1}^{n}\dot{\omega}_k M_k,
\end{aligned}\right\} \qquad (1)$$

where $\mathrm{L}(\phi) = \mathrm{d}\phi/\mathrm{d}t + U\mathrm{d}\phi/\mathrm{d}x$, t is the time, x and r denote the axial and radical coordinates, u and v are the corresponding components of the velocity, U is the axial mass flow rate and a is the stretch rate. G is a combined function of the stretch rate and the stream function; ρ, T and Y_k are respectively the mass density, temperature and mass fraction of kth species; μ, C_{pk} and M_k denote the mixture viscosity, the constant-pressure heat capacity and the molecular weight of the kth species; h_k, V_{kx} and $\dot{\omega}_k$ are respectively the specific enthalpy, the diffusion velocity in the x-direction and the molar production rate of the kth species; $\dot{q}_r$ is the volumetric radiation heat loss.

To complete the specification of the problem, the potential boundary conditions are given as

$$\left.\begin{array}{l} x = -L; \quad T = T_L, \quad Y_k = Y_{kL}, \quad G = a, \\ x = 0; \quad \mathrm{d}T/\mathrm{d}x = 0, \quad \mathrm{d}Y_k/\mathrm{d}x = 0, \quad \mathrm{d}G/\mathrm{d}x = 0, \quad U = 0, \quad a = a_0, \end{array}\right\} \tag{2}$$

where the subscript L represents the data at the burner exit and a_0 is the initial stretch rate at the stagnation plane.

For radiation calculations, the optically thin assumption has been frequently used in examining the effect of radiation on laminar flames (Liu & Rogg 1991; Sibulkin & Frendi 1990; Platt & Tien 1990). In this study, the optical thickness

$$l = \int_0^{-L} k_\lambda \mathrm{d}x \tag{3}$$

is evaluated for all the calculations, where k_λ is the gas absorption coefficient. The results show that the maximum optical thickness in the present calculations is less than 0.048, and in particular at the extinction points the maximum optical thickness is less than 0.035. Therefore, it should be justifiable to employ the simple optically thin model in the present calculation of radiative heat loss. To demonstrate the sensitivity of the numerical results to the radiation properties, two different Planck mean absorption coefficient models are used to perform the calculations. By assuming CO_2, H_2O, CO and CH_4 are the most important radiating species, the volumetric rate of radiation heat loss for the energy equation can be written as

$$\dot{q}_r = -4\sigma K_p (T^4 - T_\infty^4)\,, \tag{4}$$

$$K_p = P_{CO_2} K_{CO_2} + P_{H_2O} K_{H_2O} + P_{CO} K_{CO} + P_{CH_4} K_{CH_4}\,, \tag{5}$$

where σ is the Stefan–Boltzmann constant, and T and T_∞ are respectively the local and the ambient temperatures. K_p denotes the Planck mean absorption coefficient of the mixture, and P_i and K_i are respectively the partial pressure and Planck mean absorption coefficient of species i. Data for the Planck mean absorption coefficient of the four radiating species obtained by Tien (1968) and Kuznetsov & Sabelnikov (1990) are used to perform the calculations and the results are compared. Data given in Tien (1968) were calculated from the wide-band model and are widely accepted. We name it 'radiation model I'. On the other hand, data given in Kuznetsov & Sabelnikov (1990) were obtained experimentally and give a much lower estimation of the Planck mean absorption coefficients than radiation model I. We call it 'radiation model II' hereafter. Unless otherwise stated, the results presented in the following sections are calculated using radiation model I. The data for the Planck mean absorption

Emitting species	A_{i0}	A_{i1}	A_{i2}
CH_4	10.17015	-7.947312×10^{-3}	4.342446×10^{-7}
CO	1.565360	1.483914×10^{-2}	-2.656035×10^{-5}
CCO_2	32.44420	7.537513×10^{-2}	-1.535140×10^{-4}
H_2O	68.69480	-1.523490×10^{-1}	1.417848×10^{-4}
	A_{i3}	A_{i4}	A_{i5}
CH_4	1.048611×10^{-9}	$-2.287861 \times 10^{-13}$	0
CO	1.687980×10^{-8}	$-4.674473 \times 10^{-12}$	4.767887×10^{-16}
CCO_2	9.487940×10^{-8}	$-2.509259 \times 10^{-11}$	2.447995×10^{-15}
H_2O	-6.620996×10^{-8}	1.524150×10^{-11}	1.373456×10^{-15}

TABLE 1. Fitting coefficients for the calculation of the Planck mean absorption coefficients of the emitting species in the temperature range 300–3000 K

coefficients given by Tien are fitted by a polynomial curve

$$K_i = \sum_{j=0}^{5} A_{ij} T^j \,, \quad i = 1, 4. \tag{6}$$

The coefficients A_{ij} are tabulated in table 1.

The detailed chemical mechanism used in this study is the C_1 chemistry presented by Kee *et al.* (1985), which includes 58 elementary reactions and 18 reacting species. Nitrogen is treated as inert here. Transport properties are calculated from the CHEMKIN database (Kee *et al.* 1986). The thermal diffusion of H and H_2 is also taken into account.

By using the upwind and central finite difference scheme, the above differential equations (1) can be approximated by a set of algebraic equations of the form

$$F(\boldsymbol{V}) = 0 \tag{7}$$

at each grid point. Here $\boldsymbol{V}$ is the solution vector of $(a,\ T,\ Y_i,\ U,\ G)^T$. For an initial estimate $\boldsymbol{V}_0$ which is sufficiently close to the final solution, the above system of equations can be solved by a modified damped Newton's method following the strategy presented by Smooke (1982). However, this method becomes increasingly difficult near a turning point such as extinction. In particular, at the turning point the Jacobian of the system of equations is singular. The usual technique to alleviate this problem was developed first by Keller (1977) and later applied to flame simulations by Heinemann, Overholser & Reddien (1980) and Giovangigli & Smooke (1987). The solution vector $\boldsymbol{V}$ is considered to be a function of a new continuation variable s which is defined as the normalized arclength Δs on the temperature and strain rate plane

$$\Delta s = s - s_0 = [(T - T_0)^2 + (a - a_0)^2]^{1/2}. \tag{8}$$

Here the subscript 0 denotes the initial solution variables. Thus, the overall problem becomes one of the solution of a new set of equations

$$H(\boldsymbol{V}, s) = 0 \tag{9}$$

and the boundary condition of $a = a_0$ in (2) is replaced by the normalization condition

$$\Delta s = \frac{\mathrm{d}T}{\mathrm{d}s}[T(s) - T(s_0)] + \frac{\mathrm{d}a}{\mathrm{d}s}[a(s) - a(s_0)]. \tag{10}$$

With an initial solution vector of $\boldsymbol{V}_0$ at s_0, a new solution estimate can be obtained by using

$$\boldsymbol{V}(s+\delta s) = \boldsymbol{V}(s_0) + \frac{\mathrm{d}\boldsymbol{V}}{\mathrm{d}s}\delta s. \tag{11}$$

Here the Jacobian $\mathrm{d}\boldsymbol{V}/\mathrm{d}s$ is non-singular.

In theory, this procedure overcomes the singularity problem of the Jacobian. However, in practice, the new solution estimate from (11) occasionally makes the computation difficult to converge. Since at the turning point the singular Jacobian occurs at the strain rate coordinates, (7) is solved by a given stretch rate at the stagnation plane. However, the Jacobian at the temperature coordinate is not singular at the turning point. This suggests that the singularity problem could be removed simply by respectively choosing the strain rate and the stagnation temperature as the independent continuation variables in the region far from the turning point and in the region near the turning point. In practice, near the extinction limit, $\mathrm{d}a/\mathrm{d}s$ in (10) is set to zero; otherwise, $\mathrm{d}T/\mathrm{d}s$ is set to zero (away from the extinction limit). This is the strategy used in this work. The present calculations show that these procedures can proceed smoothly through a whole solution branch.

3. Radiation cooling and temperature dip

Axial temperature profiles of the gaseous mixture of two symmetric counterflow methane–air premixed flames were measured by Liu *et al.* (1986). To examine the effects of radiation cooling and demonstrate the validity of the present theoretical models, especially the radiation model, a comparison between the measured temperature and the prediction is made. The boundary conditions used in the calculation are identical to those of the experiment. The separation distance between burners is 2 cm here. The velocity at the burner exit plane is kept at the constant value of 20 cm s^{-1}. The volumetric percentages of methane in air, Ω, are 6.53 and 5.88.

Since the temperature measurement was carried out using a thermocouple of 0.05 mm diameter, to compare the prediction with the experimental data, a radiation correction of the measured temperature has been made here according to the expression suggested in Liu *et al.* (1986):

$$T_c = T_m + \frac{\epsilon\sigma d}{2\lambda}(T_m^4 - T_\infty^4)\,, \tag{12}$$

where ϵ, d and λ are respectively the coating emissivity, junction diameter and gas thermal conductivity. T_c and T_m are respectively the corrected temperature and the measured temperature.

The corrected axial temperature profiles and predicted axial temperature profiles are compared in figure 2. It can be seen that both the experimental data and the predicted results display a temperature dip with the minimum for each curve at the stagnation plane. Since the rate of radiation heat loss is proportional to the volume fractions of the radiating gases, as shown in figure 2, the magnitude of this temperature dip increases as the separation distance between the twin flames increases. As a result, this temperature dip will induce conductive heat loss from the flame region to the stagnation plane region. Therefore, the radiation cooling mechanism in this twin premixed flame configuration consists of two parts: a direct radiation heat loss through gas emitting within and upstream of the reaction zone and an indirect conduction heat loss due to the existence of the temperature gradient caused by stronger radiative heat loss downstream of the reaction zone. At higher

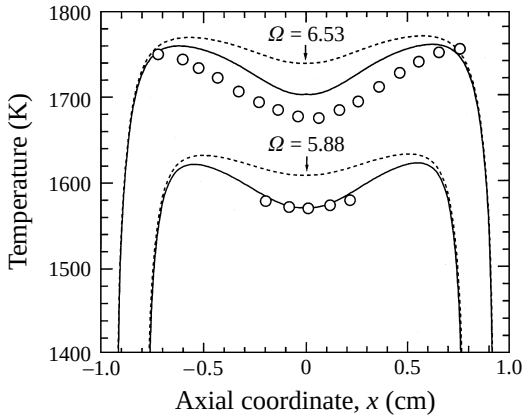

FIGURE 2. Comparison of axial temperature profiles between experiment and prediction for two typical methane percentages, Ω, in air: ○, experiment (Liu *et al.* 1986); ——, radiation model I; - - - - -, radiation model II.

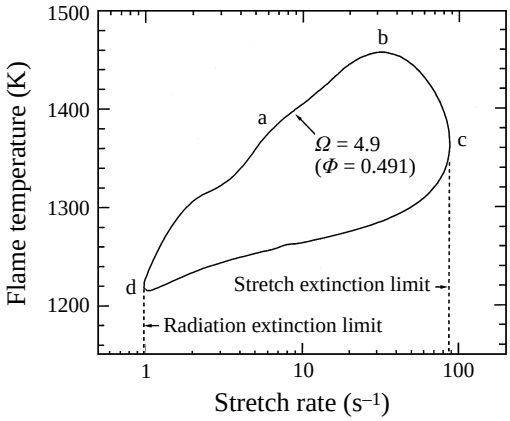

FIGURE 3. Flame temperature profile plotted as a function of stretch rate for $\Omega = 4.9$.

stretch rates, the indirect conduction heat loss plays an important role in flame cooling, since the reaction zone is very thin and diffusion of emitting species is suppressed due to the short convection time. At low stretch rates, however, direct radiation heat loss within and upstream of the reaction zone may become very important since the flame thickens and the diffusion process becomes dominant. These behaviours will be discussed in detail in the next Section.

It can be also seen that radiation model II greatly underestimates the effects of radiation heat loss compared to radiation model I and the experiment. Although there are some discrepancies between the experimental data and the results predicted by radiation model I, considering the errors due to the radiation correction of the experimental data and the use of the simple optically thin assumption, the agreement is quite good.

4. Extinction mechanism near the lean limit

Figure 3 shows the variation of the flame temperature (maximum temperature) with stretch rate for methane percentage in air $\Omega = 4.9$ (Φ denotes the equivalence ratio).

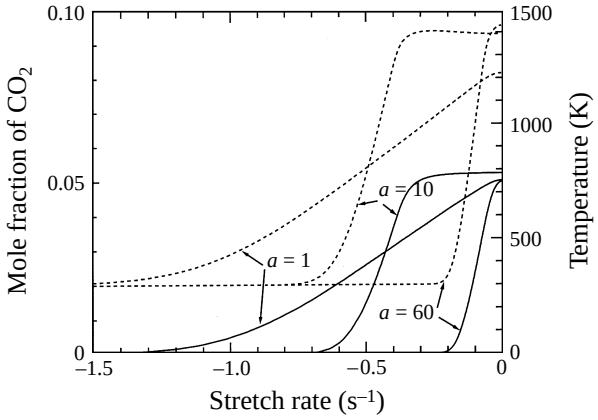

FIGURE 4. Axial distributions of temperature (- - - - -) and mole fraction of CO_2 (——) for $\Omega = 4.9$, at various stretch rates a (in s^{-1}).

Starting from point a (corresponding to a stretch rate of about 6.0 s^{-1}), the peak flame temperature increases dramatically with the increase of stretch rate. This increase of temperature is attributed to the decreased effect of radiation loss (this will be shown in figure 6) and to the Lewis number effect. Since the Lewis number of a fuel-lean methane–air mixture is slightly less than unity, an increase of stretch rate causes a larger energy gain due to the increase of the deficient reactant through diffusion than the energy loss through conduction. As shown in figure 3, at the stretch rate of 32 s^{-1} (point b), the peak flame temperature reaches its maximum. With a further increase of stretch rate, the flame is pushed towards the stagnation plane and chemical reactions cannot be completed because of the reduced residence time. As a result, the peak flame temperature decreases and this eventually leads to extinction at point c. This extinction is caused by the stretch effect, so we call it the 'stretch extinction' hereafter (Maruka *et al.* 1996; Guo *et al.* 1996). On the other hand, a decrease of stretch rate from point a results in a continuous drop of the peak flame temperature. At point d, a new extinction point emerges. Since this extinction is mainly caused by radiative heat loss, we name it the 'radiation extinction limit', to distinguish it from the stretch extinction limit mentioned above. As shown in figure 3, the curve of the peak flame temperature versus the stretch rate is O-shaped. The upper half of the curve, dabc, represents the stable flame branch which can be observed in the laboratory. On the other hand, from knowledge of the 'fold bifurcation' (Thompson & Stewart 1986), we know that the lower half of the curve, cd, is the physically unstable flame branch. Therefore, there exists only one stable flame at each stretch rate between the stretch and the radiation extinction limits for $\Omega = 4.9$.

To demonstrate the detailed physical process of the extinction, the distributions of temperature and CO_2 mole fraction in the axial direction for $\Omega = 4.9$ are plotted in figure 4 for three typical stretch rates. At a large stretch rate of 60 s^{-1}, it can be seen that reaction zone is pushed to the stagnation plane ($x = 0$). The flame will be extinguished at a larger stretch rate through incomplete combustion. As the stretch rate decreases to 10 s^{-1}, the flame moves upstream and thickens. We know that the radiation heat loss depends primarily on the concentration of the radiating species (CO_2 and H_2O) and the temperature. Figure 4 clearly shows that a decrease of stretch rate causes a dramatic change of the distributions of these parameters. When the stretch rate further decrease to 1.0 s^{-1}, the increase of radiation heat loss due to

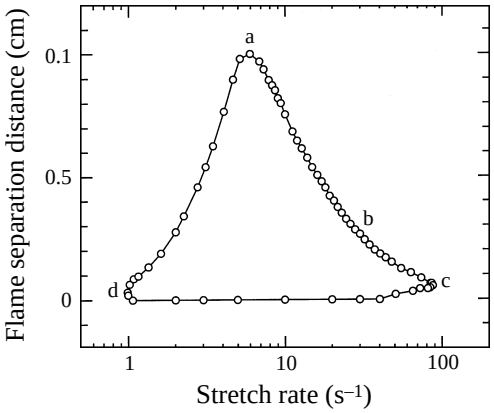

FIGURE 5. Flame separation distance plotted as a function of stretch rate for $\Omega = 4.9$ ($\Phi = 0.491$).

the flame thickening and the weakening of the Lewis number effect in enhancing the combustion both lead a rapid decrease of flame temperature.

The flame separation distance corresponding to figure 3 is shown in figure 5. The flame position is defined by the location of the maximum CH concentration. It can be seen that at point a the flame separation distance reaches its maximum. An increase or decrease of the stretch rate results in a decrease of the flame separation distance. The increase in flame separation distance with decreasing stretch rate is well known. However, the decrease of flame separation with decreasing stretch rate is new. The reason for the decrease of the flame separation distance at low stretch rate is due to the radiation heat loss. At point a, there is a large temperature dip in the temperature profile. Hence, as mentioned in the last section, the indirect conduction heat loss downstream of the reaction zone reduces the flame temperature and causes the flames to narrow their separation distance. On the other hand, near the extinction point d, the flame moves almost to the stagnation plane. The flame separation distance is very small and no temperature dip exists behind the reaction zone. Thus, the indirect conduction heat loss can become negligible. However, the direct radiation heat loss within and upstream of the reaction zone becomes increasingly important as the stretch rate decreases. At the stretch rate of 0.99 s^{-1}, the flame is extinguished because of incomplete combustion caused by the direct radiation heat loss. Therefore, the direct mechanisms for stretch extinction and radiation extinction of the stretched flames are very different, although they share a common phenomenon of incomplete combustion near the extinction limits.

To quantitatively evaluate the effect of radiation heat loss, a radiation distribution function is introduced:

$$f_r(x) = \int_{-\infty}^{x} \dot{q}_r \mathrm{d}x \Big/ \int_{-\infty}^{0} \dot{q}_c \mathrm{d}x \,, \tag{13}$$

where $f_r(x)$ is the radiation distribution function, and $\dot{q}_r$ and $\dot{q}_c$ are respectively the rate of volumetric radiation heat loss and chemical heat release. Thus the numerator in (13) denotes the integration of radiation loss from the left-hand boundary to the location x and the denominator denotes the total chemical heat release rate in the left half of the domain. Therefore, $f_r(x)$ represents the proportion of radiation heat loss rate on the left-hand side of location x in the total chemical heat release rate, which we shall call the 'radiation fraction'. As x approaches zero, $f_r(0)$ denotes the total radiation fraction in the total chemical heat release. The variation of the total

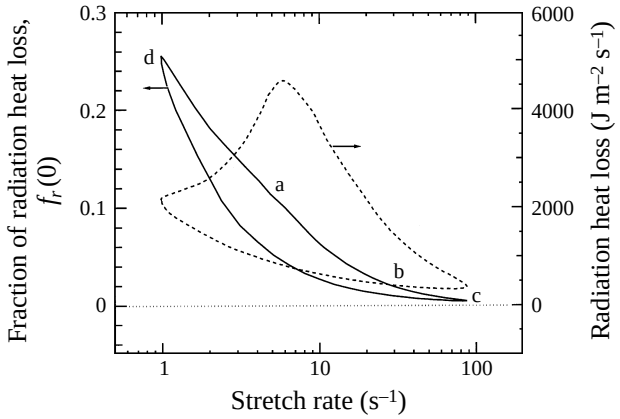

FIGURE 6. Radiation fraction, $f_r(0)$, plotted as a function of stretch rate for $\Omega = 4.9$ ($\Phi = 0.491$).

radiation fraction with stretch rate for $\Omega = 4.9$ is shown in figure 6. At the stretch extinction limit (point c), the total radiation fraction is less than 1%. At point a, where the flame separation distance reaches its maximum, the total radiation fraction increases to 12%. This radiant heat loss is so high that the flame loses its ability to propagate upstream. A further decrease of stretch rate results in a decrease of the flame separation distance (see figure 5) and a dramatic increase of the total radiation fraction. At the radiation extinction limit (point d), the total rate of radiative heat loss reaches as much as 25% of the total chemical heat release rate. Therefore, the stretch extinction and the radiation extinction occur at two different extremes.

The dashed line in figure 6 represents the total radiation heat loss rate. By comparing figure 6 with figure 5, it can be clearly seen that the total radiation heat loss rate increases with the increase of the flame separation distance (curve abc in figure 5). At point a, both the flame separation distance and the total radiation heat loss rate reach their maximum values. Although a further decrease of the stretch rate causes an increase of the total radiation fraction, the total radiation heat loss rate still decreases due to the decrease of the flame separation distance. The increase of the total radiation fraction with decrease of the stretch rate is partly attributed to the decrease of the total chemical heat release rate. As the stretch rate goes down, the mass burning rate decreases and thus leads to a decrease of the chemical heat release rate, since the chemical heat release rate depends on the mass burning rate. On the other hand, since the rate of radiation heat loss depends on the volume and temperature of the emitting species, a decrease of the stretch rate leads to an increase of the total radiation heat loss rate if the flame separation distance does not change. To compensate for the decrease of the chemical heat release rate and to reduce radiation heat loss, the flames have to adjust their location to narrow their separation. In addition, for methane–air flames, the Lewis number effect plays an increasingly important role in enhancing chemical reactions as the reaction zone moves towards the stagnation plane. Therefore, strictly speaking, the emergence of the radiation extinction limit is the result of the competition between the radiation effect and the Lewis number effect.

To demonstrate the differences in the distribution of the radiation heat loss rate over the flame at different stretch rates, variations of the radiation distribution function and the chemical heat release rate with axial distance are plotted in figure 7. For a stretch rate of $a = 10$ s^{-1}, the rate of radiation heat loss upstream of and within the

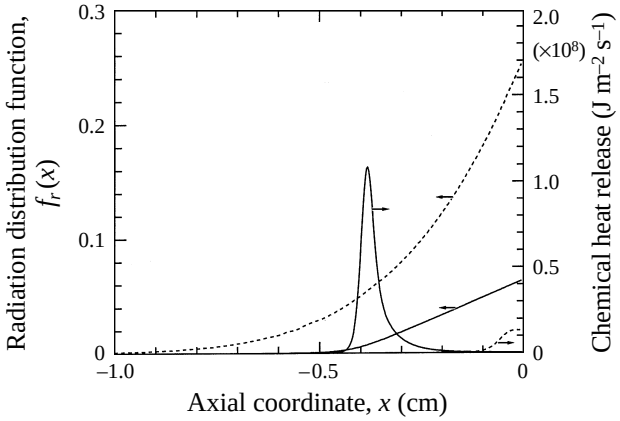

FIGURE 7. Radiation distribution function $f_r(x)$ and chemical heat release for stretch rates $a = 10$ s^{-1} (——) and $a = 1.0$ s^{-1} (- - - - -).

reaction zone, which is directly responsible for flame temperature reduction, is less than 1% of the total chemical heat release rate. Thus, most of the radiation heat loss occurs downstream of the reaction zone. However, for a stretch rate of $a = 1.0$ s^{-1}, radiation heat loss is important both upstream of and within the reaction zone. Thus, direct radiation heat loss is the mechanism inducing the radiation extinction at low stretch rate.

Profiles of the peak flame temperature calculated using radiation model I near the lean flammability limit of counterflow premixed flames are shown in figure 8(*a*). It can be seen that each stable flame in the range of percentage of volumetric fuel to air between 4.23 and 4.6 has two extinction limits: a radiation limit and a stretch limit. Peak flame temperature profiles calculated using radiation model II are shown in figure 8(*b*). Although both the stretch limit and the radiation limit are extended due to the underestimation of radiation heat loss, these two extinction limits still exist. Near the lean limit, results of both radiation models show that the peak temperature curves are O-shaped and there exists only one stable flame at each stretch rate between the two extinction limits (the upper branch).

5. Flame structure and extinction mechanism away from the lean limit

In order to fully understand the interactions between the radiation effect and the stretch effect and to establish the connection between the stretched flame and the planar propagating flame, an investigation of the flame structure and the extinction mechanism at higher equivalence ratio Φ and low stretch is necessary. A comparison between the peak flame temperature profiles at fuel percentages 5% and 4.9% is given in figure 9. For $\Omega = 4.9$ ($\Phi = 0.491$), as described above, there are two extinction limits and the profile is a closed O-shaped curve. However, for $\Omega = 5.0$ ($\Phi = 0.501$), the O-shaped curve opens up and becomes 'mushroom shaped'. As a result, the stable branch dabc at $\Omega = 4.9$ divides into two branches a′b′c′ and e′d′. As shown in figure 9, all the turning points c′, d′ and e′ are the simple fold bifurcation points. From the study of the fold bifurcation (Thompson & Stewart 1986), we know that the turning point is a separation point between the stable branch and the unstable branch. On the other hand, we also know that a′b′c′ is the temperature curve of the 'normal' stable flame, corresponding to curve abc in the case $\Omega = 4.9$. Therefore, branch c′d′

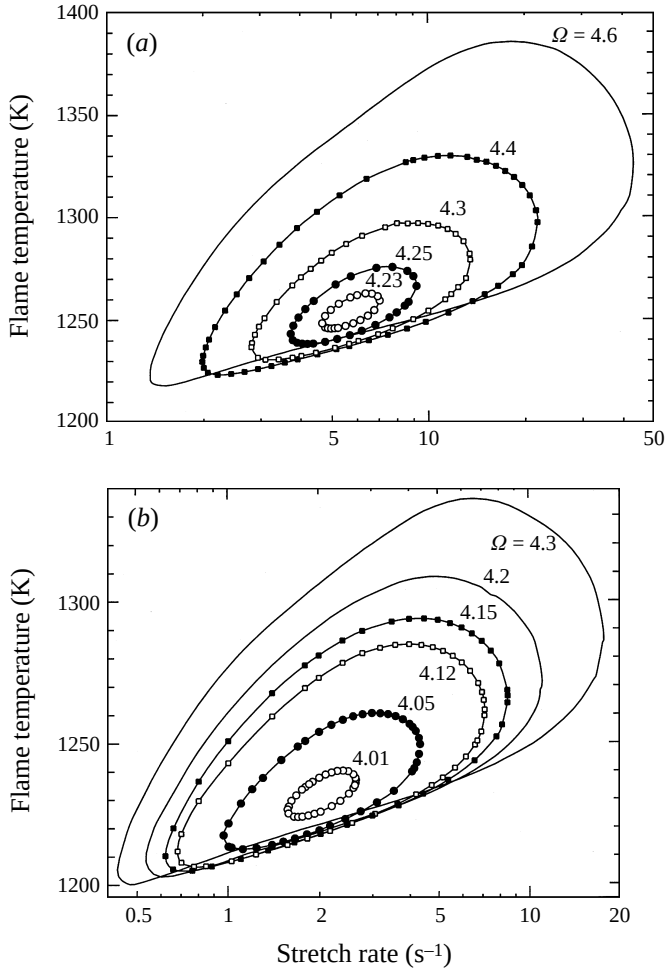

FIGURE 8. Flame temperature profiles plotted as a function of stretch rate for various fuel percentages in air with (*a*) radiation model I; (*b*) radiation model II.

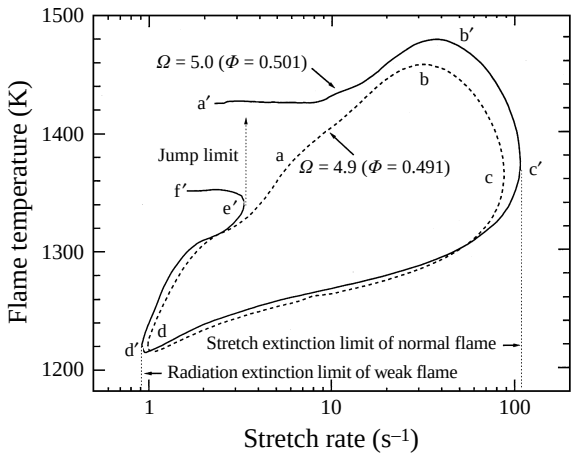

FIGURE 9. Comparison of flame temperature profiles between $\Omega = 4.9$ and $\Omega = 5.0$.

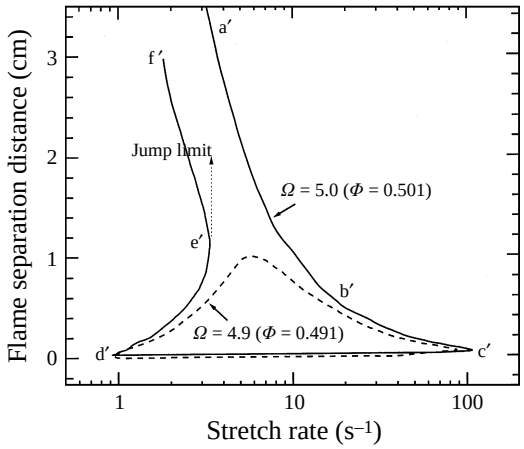

FIGURE 10. Comparison of flame separation distances between $\Omega = 4.9$ and $\Omega = 5.0$.

represents the temperature curve of physically unstable flames and curve d′e′ denotes the low-temperature physically stable flames. Hereafter, we call curve d′e′ the 'weak flame' branch because its temperature is lower than the 'normal flame' (a′b′c′). Again, curve f′e′ represents another physically unstable flame branch. For a normal flame, an increase of stretch rate enhances chemical reaction and reduces the convective residence time. The flame reaches its maximum temperature at point b′ and quenches at point c′. This behaviour of the flame is the same as that for $\Omega = 4.9$. However, unlike the case $\Omega = 4.9$, as the stretch rate goes down, the flame temperature does not decrease significantly but tends towards a constant value. This implies that the normal flame will not be extinguished as the stretch rate further decreases and point a′ can be extrapolated to zero stretch rate. Therefore, the normal flame for $\Omega = 5.0$ also has only one limit, the stretch extinction limit. It is only in this case that a normal flame can be reduced to a planar propagating flame in the limit of zero stretch. For $\Omega \leqslant 4.9$, the flame is strengthened by the stretch due to the Lewis number effect and it cannot be extended to the corresponding planar propagating flame.

The low-temperature stable flame (d′e′) exists within the range of stretch rate of the normal flame. As the stretch rate goes down, radiation extinction occurs at point d′. On the other hand, as the stretch rate goes up, the flame temperature increases rapidly. At point e′, the temperature gradient becomes infinite, showing a jump phenomenon. Since there is no solution for the weak flame as the stretch rate further increases, point e′ can be defined as a 'jump limit', at which the weak flame temperature suddenly jumps and the weak flame becomes a normal flame instantaneously. In addition, the unstable branch e′f′ can also be extrapolated to zero stretch rate. Moreover, a′ and f′ at zero stretch rate correspond respectively to the stable and the unstable solutions of the one-dimensional planar propagating flame.

A comparison of the flame separation distances between the results for $\Omega = 4.9$ and $\Omega = 5.0$ is shown in figure 10. The distinction between these two cases is obvious. For $\Omega = 4.9$, there exists a maximum flame separation distance. The right half can be considered as a normal flame branch and the left half is the radiation-controlled flame branch. These two branches merge at the point of the maximum separation distance. However, for $\Omega = 5.0$, the flame separation distance of the normal flame (a′b′c′) increases monotonically with the decrease of the stretch rate. In the limit of zero stretch, it is expected that the flame separation becomes infinite and the twin

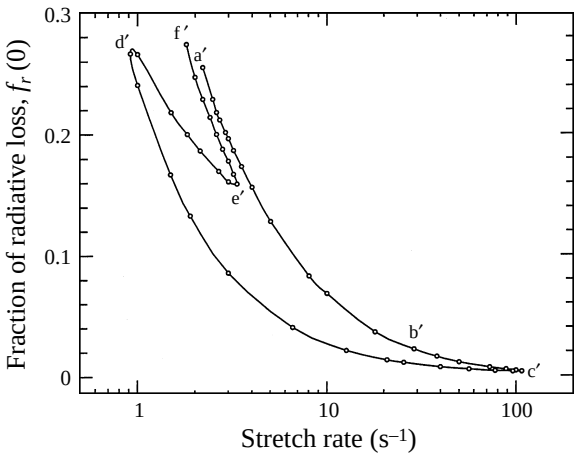

FIGURE 11. Radiation fraction, $f_r(0)$, plotted as a function of stretch rate for $\Omega = 5.0$.

flames reduce to two independent plane propagating flames. On the other hand, at the weak flame branch (d′e′), the flame separation distance increases with the increase of the stretch rate. At jump point e′, the rate of increase of the flame separation distance becomes infinite, indicating that the weak flame will propagate upstream suddenly. Unlike the case $\Omega = 4.9$, the normal flame branch does not merge with the weak flame branch. Even so, at the radiation extinction limit of the weak flame and the stretch extinction limit of the normal flame, extinction still occurs by way of incomplete combustion with the flame being pushed to the stagnation plane. At the jump limit, however, the flames separate at a finite distance and no incomplete combustion occurs.

Figure 11 shows the fraction of total radiation heat loss relative to chemical heat release. On the normal flame branch (a′b′c′), the radiation fraction increases quickly with the decrease of stretch rate due to the increase of the flame separation distance. At point a′, the radiation fraction increases to 25%. On the other hand, at the radiation extinction limit of the weak flame, the radiation fraction is as high as 27%. As the stretch rate goes up, the radiation fraction decreases. The reason is that an increase of the strain rate enhances chemical reaction and results in an increase of the mass burning rate. At the jump point e′, the radiation fraction reaches its minimum. This is why the weak flame has enough potential to jump up to the normal flame branch. It should be noted that although the radiation fractions at point d′ and a′ are comparable, the extent of radiation heat loss contributing to flame cooling upstream of the flame zone at point a′ is much larger than that at point d′.

A comparison of the radiation distribution functions and chemical heat release rate between the normal flame and the weak flame at the same stretch rate is given in figure 12. For the normal flame, the mass burning rate is very high. Although the radiation fraction is as high as 20% for the normal flame, the direct radiation heat loss within and upstream of the reaction zone is only about 1%. Therefore, the contribution of radiation heat loss to flame cooling is mainly through the indirect heat conduction. This effect on flame temperature reduction is very weak. However, for the weak flame, although the radiation fraction is less than that of the normal flame, the direct radiation heat loss within and upstream of the reaction zone is far greater than that of the normal flame. This direct radiation heat loss affects the flame temperature considerably and thus results in a low flame temperature and a narrow flame separation distance.

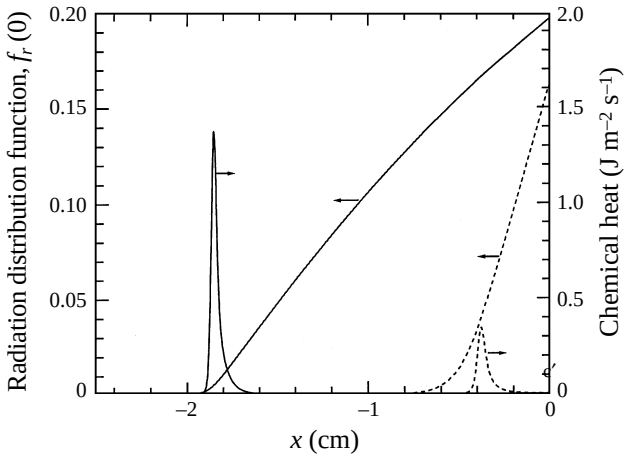

FIGURE 12. Radiation distribution function $f_r(x)$ and chemical heat release for a normal flame (——) and a weak flame (- - - - -) at stretch rate $a = 3$ s^{-1}.

The effect of radiation on flame structure can be easily understood by comparing the results of the adiabatic flame with those of the non-adiabatic flame. Figures 13(*a*) and 13(*b*) respectively show a comparison of flame temperatures between adiabatic and non-adiabatic flames calculated using radiation models I and II. In figure 13(*a*), it can be clearly seen that there is only one stable flame at each stretch rate for the adiabatic flame. Radiation affects flame structure dramatically at low stretch rate while has little impact on the flame temperature at high stretch rate, especially near the stretch extinction point. Although radiation is greatly underestimated by radiation model II, figure 13(*b*) also shows the existence of two stable flames. Therefore, the conclusion can be drawn that the emergence of a weak stable flame is the result of the interaction between the radiation effect and the stretch effect at high equivalence ratio.

6. Brief summary

To help understanding of the phenomena described in last two Sections, a brief summary is given here. We know that the Lewis number of a methane–air mixture is less than unity. Thus, a moderate stretch will strengthen the flame but a large stretch will quench it. For an equivalence ratio less than the standard flammability limit, as can be seen in figure 8, a moderate stretch rates enhances the combustion and makes the flame stable. A large stretch rate quenches the flame due to stretch-induced incomplete combustion (stretch extinction). On the other hand, at a sufficiently low stretch, the increase of radiation heat loss due to flame thickening and the weakening of the combustion enhancement due to the Lewis number effect also quench the flame (radiation extinction). These results are shown in figure 8 by the O-shaped isola. This isola indicates that below the standard lean limit the mixture can be made to burn by imposing a moderate stretch.

What happens to the flame when the mixture equivalence ratio is higher than the standard flammability limit? For the one-dimensional propagating flame, we know that there are two solutions for a given mixture strength, one of which is stable and the other unstable. For the counterflow flame we also know that there is a stretch extinction limit at large stretch. The question is what happens at moderate stretch rates. Figure 9 shows the answer. For $\Omega = 5.0$, the flame branch opens up at the

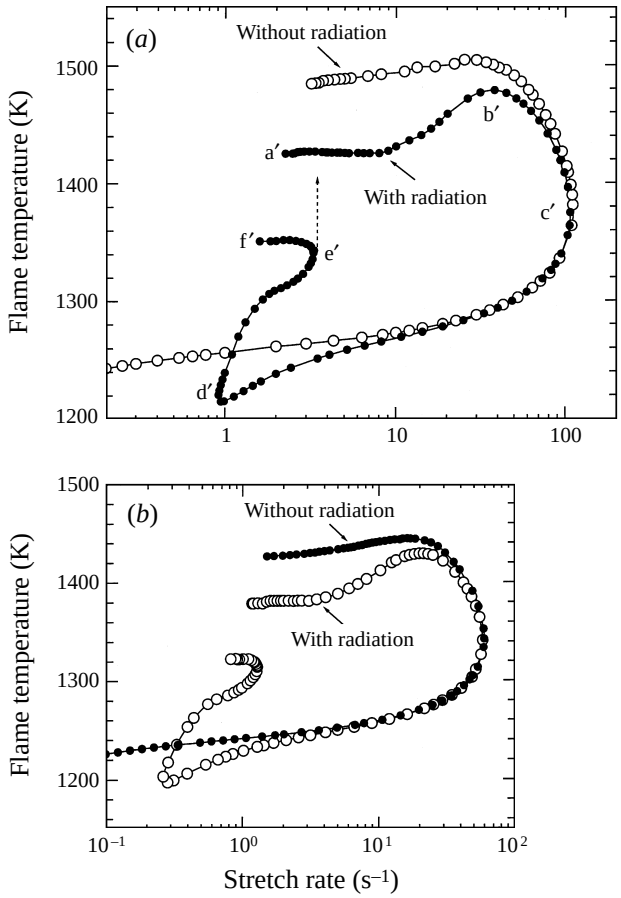

FIGURE 13. Comparison of flame temperature profiles between adiabatic flame and non-adiabatic flames for $\Omega = 5.0$: (*a*) radiation model I; (*b*) radiation model II.

middle point (e′) of the upper stable branch. Therefore, the stable branch divides into two stable flame branches: the weak flame branch on which the flame can survive from the radiation limit (point d′) to the opening point e′, and the normal flame branch on which the flame can survive from the stretch extinction limit to zero stretch rate. In figure 9, e′f′ is an unstable branch. The extrapolations of a' and f' to zero stretch respectively yield the stable and unstable solutions for the one-dimensional planar propagating flame. Therefore, figure 9 has established a clear relation between the stretched flame and the one-dimensional planar propagating flame.

7. Comparison with experiment and the extinction curve

The variation of the two extinction limits with the equivalence ratio shown in figure 8 is plotted in figure 14. Numerical calculations are conducted using the two different radiation models. Experimental data were obtained under the conditions of normal gravity and microgravity (Maruta *et al.* 1996; Law *et al.* 1986). It can be seen that, for an adiabatic flame, the extinction limit decreases monotonically with the decrease of the equivalence ratio. However, for a non-adiabatic flame, numerical results obtained using the two different radiation models show that there are two branches of extinction

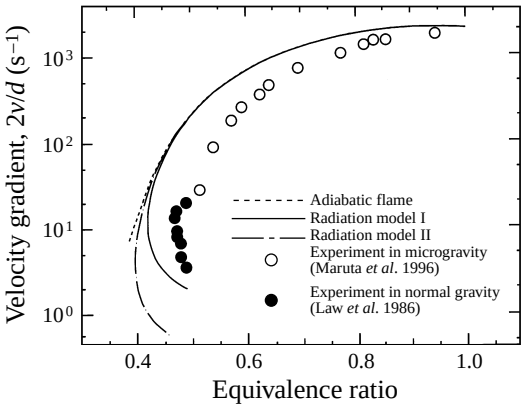

FIGURE 14. Comparison of extinction limits as a function of the equivalence ratio obtained by experiments and numerical calculations using the two different radiation models

limits. As shown in figure 14, the upper branch is the stretch extinction branch while the lower branch represents the radiation extinction branch. The merging point of the two branches denotes the flammability limit of stretched flames. Figure 14 also shows that radiation heat loss has almost no effect on the stretch extinction limit for an equivalence ratio larger than 0.5. For equivalence ratios below 0.5, however, radiation dramatically affects both the stretch extinction limit and the radiation extinction limits. Since the effect of radiation is underestimated by radiation model II, the predicted flammability limit of stretched flames is smaller than that calculated by radiation model I. In addition, the experimental data also show the existence of the radiation branch. Although there is some discrepancy between the experimental data and the prediction, considering the use of a simple model of radiation and the effect of burner diameter in the experiment, the agreement can be considered to be quite good.

A general graph showing both the extinction limits and the jump limits in figures 8 and 9, for stretched methane–air premixed flames is shown in figure 15(*a*). Since the graph exhibits a shape similar to the letter G, we name it the 'G-curve'. On this G-curve, branches AB and BC are respectively the stretch extinction branch and radiation extinction branch shown in figure 14. Point B is the flammability limit of stretched flames (inferior limit). Curve CE represents the radiation limits of normal flames, showing that a normal flame will not extinguish on the right-hand side of line CE by radiation as the stretch rate goes down. Curve CF represents the radiation branch of the weak flame. DG denotes the jump branch from the weak flame to the normal flame. Simply speaking, the normal flame can exist in the region bounded by curve ABCE (of course, there is also a right-hand limit on the fuel-rich side). In region GDCF, the weak flame can co-exist with the normal flame. The radiation limit of the weak flame decreases with the increase of equivalence ratio. It has its minimum near the equivalence ratio of 0.85. A further increase of equivalence ratio results in an increase of the radiation extinction limit. The variation of the jump limits of the weak flame with the equivalence ratio behaves similarly to that of its radiation extinction branch.

It should be noted that neither the linear extrapolation of the stretch extinction branch (AB) nor the linear extrapolation of the radiation extinction branch (BCF) to the zero stretch rate yields a correct prediction of the standard flammability limit of a one-dimensional planar propagating flame. Figure 15 shows that only for equivalence

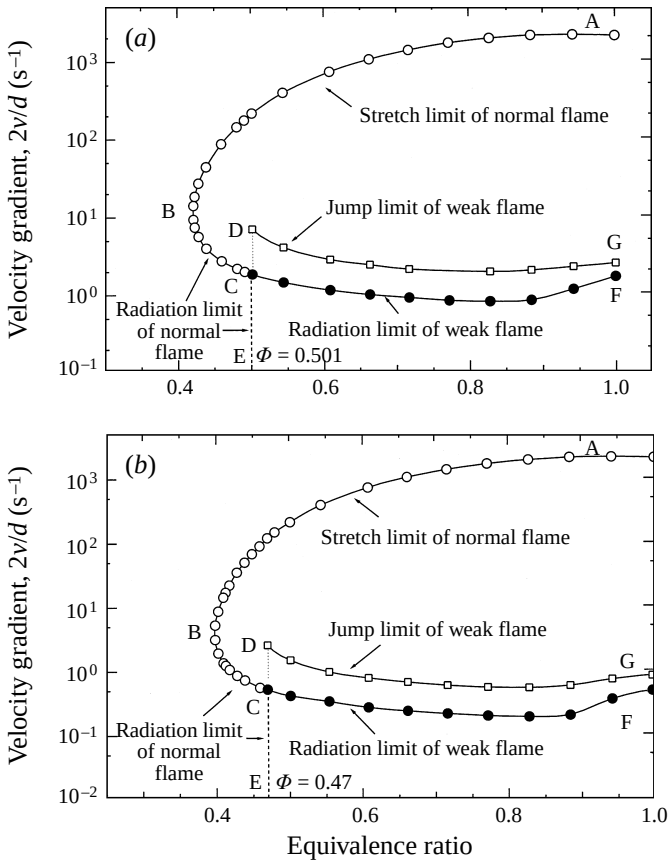

FIGURE 15. A G-shaped graph showing both the extinction limits and jump limits as well as the flammability of the stretched methane–air premixed flame calculated by (*a*) radiation model I, (*b*) radiation model II.

ratio larger than 0.5, can a stretched flame be extended to zero stretch and reduced to the planar propagating flame. The experimental study conducted by Ronney (1988) showed that the standard flammability limit of a methane–air mixture is 0.51. As shown in figure 15, the present prediction of the flammability limit of a planar propagating flame is 0.5, which is very close to the experimental value. The G-curve also shows that the flammability limit of a stretched flame is far less than that of a one-dimensional planar propagating flame due to the effect of the Lewis number.

The extinction curve obtained by using radiation model II is shown in figure 15(*b*). Although there are some quantitative differences in the limits from those given in figure 15(*a*), the existence of the G-curve remains unchanged. Therefore, it can be concluded that the results obtained in this study do not depend on a specific simple radiation model. Instead, the results correctly reveal the physical phenomena inherent in stretched premixed flames with radiative heat loss.

8. Conclusion

Flame regimes, extinction limits and the flammability limit of stretched premixed methane–air flames with radiation heat loss are studied numerically with detailed chemistry. The present results reproduced well the temperature dip observed experi-

mentally. Furthermore, the present results clearly show that radiation heat loss has a significant effect on flame structure and the extinction limit through two different mechanisms; indirect heat conduction loss downstream of the reaction zone and direct radiation heat loss within and upstream of the reaction zone. At high stretch rate, indirect conduction heat loss is the main factor affecting the flame temperature. At low stretch rate, however, the direct radiation heat loss is the dominant mechanism for flame extinction.

The results further show that, for an equivalence ratio lower than the standard flammability limit, the flame temperature profile is O-shaped and there are two extinction limits for each stable flame; a radiation limit at low stretch rate and a stretch limit at high stretch rate. The radiation limit is the result of competition between the radiation effect and the Lewis number effect. The results show that below the standard flammability limit the mixture can be made to burn by imposing a moderate stretch for Lewis number less than unity.

It is also found that for an equivalence ratio larger than 0.5, the flame temperature profile opens up and becomes a mushroom-shaped curve. There are two stable flames, a normal flame and a weak flame, coexisting at the same stretch rate between the radiation extinction limit and the jump limit. The normal flame has only one limit, the stretch extinction limit. The weak flame has two distinct limits; a radiation extinction limit and a jump limit indicating a sudden change from a weak flame to a normal flame. The emergence of the weak flame is due to the interaction between radiation and stretch. A G-shaped curve showing both the extinction limits and jump limits as well as the flammability of stretched premixed methane–air flames, is presented. It is shown that although the treatment of radiation heat loss affects considerably the values of extinction limits, the existence of the G-shaped curve is physical for stretched premixed flames with radiation heat loss. It is found that the flammability limit of stretched methane–air premixed flames is far lower than that of one-dimensional planar propagating flames because the Lewis number is less than unity. This limit will become narrower with increasing Lewis number. It is also shown that neither the linear extrapolation of the stretch extinction branch nor the linear extrapolation of the radiation extinction branch to the zero stretch limit can correctly predict the flammability limit of the one-dimensional planar propagating flame. The present results agree well with available experimental data. Although the existence of the weak flame has not been observed in previous experiments, it is expected that this finding would be confirmed in future experiments conducted in microgravity.

In a future study, stable regions of the weak flames and the stability analysis of all the stable solution branches should be addressed.

The authors would like to extend their thanks to Professor Takashi Niioka, Professor Osamu Inoue, Professor Toshiyuki Hayase and Dr Yuji Hattori in the Institute of Fluid Science of Tohoku University for interesting suggestions and discussions. The authors also thank the reviewers' efforts to clarify the presentation

REFERENCES

Chao, B. H., Law, C. K. & Tien, J. S. 1990 *Twenty-Third Symp. (Intl) on Combustion*, pp. 523–531. The Combustion Institute.

Dixon-Lewis, G. 1990 *Twenty-Third Symp. (Intl) on Combustion*, pp. 305–324. The Combustion Institute.

Egerton, A. & Thabet, S. K. 1952 *Proc. R. Soc. Lond.* A **211**, 445–471.

Giovangigli, V. & Smooke, M. D. 1987 *Combust. Sci. Tech.* **53**, 23–49.

Guo, H., Ju, Y., Maruta, K., Niioka, T. & Liu, F. 1996 Radiation extinction limit for counterflow premixed fuel-lean methane–air flame. *Combust. Flame* (to appear).

Heinemann, R. F., Overholser, K. A. & Reddien, G. W. 1980 *AIChE J.* **26**, 725–733.

Kee, R. J., Miller, J. A., Evans, G. H. & Dixon-Lewis, G. 1988 *Twenty-Second Symp. (Intl) on Combustion*, p. 1479. The Combustion Institute.

Kee, R. J., Grear, J. F., Smooke, M. D. & Miller, J. A. 1985 *Sandia Rep.* SAND85-8240.

Kee, R. J., Dixon-Lewis, G., Warnatz, J., Coltrin, M. E. & Miller, J. A. 1986 *Sandia Rep.* SAND86-8246.

Keller, H. B. 1977 *Application of Bifurcation Theory* (ed. P. Rabinowitz). Academic.

Kuznetsov, V. R. & Sabelnikov, V. A. 1990 *Turbulence and Combustion*, pp. 207–208. Hemisphere. The Combustion Institute.

Law, C. K. & Egolfopoulos, F. N. 1990 *Twenty-Third Symp. (Intl) on Combustion*, pp. 413–421. The Combustion Institute.

Law, C. K., Zhu, D. L. & Yu, G. 1986 *Twenty-First Symp. (Intl) on Combust.*, p. 1419. The Combustion Institute.

Lakshmisha, K. N., Paul, P. J. & Mukunda, H. S. 1990 *Twenty-Third Symp. (Intl) on Combustion*, pp. 523–531. The Combustion Institute.

Liu, G. E., Ye, Z. Y. & Sohrab S. H. 1986 *Combust. Flame* **64**, 193–201.

Liu, Y. & Rogg, B. 1991 In *Heat Transfer in Radiating and Combusting Systems* (ed. M. G. Carvalho, F. Lockwood, & J. Taine), pp. 114–127. Springer.

Maruta, K., Yoshida, M., Ju, Y. & Niioka, T. 1996 *Twenty-Sixth Symp. (Intl) on Combustion*, to appear. The Combustion Institute.

Platt J. A. & Tien J. S. 1990 *Chemical and Physical Processes in Combustion, 1990 Fall Technical Meeting, Easten Section of the Combustion Institute.*

Ronney, P. D. 1988 *Twenty-Second Symp. (Intl) on Combustion*, pp. 1615–1623. The Combustion Institute.

Ronney, P. D. & Wachman, H. Y. 1988 *Combust. Flame* **62**, 107–115.

Sibulkin, M. & Frendi, A. 1990 *Combust. Flame* **82**, 334–345.

Smooke, M. D. 1982 *J. Comput. Phys.* **48**, 72–105.

Sohrab, S. H. & Law, C. K. 1984 *Intl J. Heat Mass Transfer* **27**, 291–300.

Spalding, D. B. 1957 *Proc. R. Soc. Lond.* A **240**, 83–100.

Thompson, J. M. T. & Stewart, H. B. 1986 *Nonlinear Dynamics and Chaos*, pp. 110–120. John Wiley and Sons.

Tien, C. L. 1968 *Adv. Heat Transfer* **5**, 253–324.

Tien, J. H. & Matalon, M. 1991 *Combust. Flame* **84**, 238–248.

Tien, J. S. 1986 *Combust. Flame* **65**, 31–34.

Tsuji, H. 1983 *JSME-ASME Joint Thermal Engng Conf.* p. 11.